Research Article

Shalina Sheik Muhamad, Jaharah A. Ghani*, Che Hassan Che Haron, and Hafizal Yazid

Cryogenic milling and formation of nanostructured machined surface of AISI 4340

https://doi.org/10.1515/ntrev-2020-0086
received September 23, 2020; accepted October 18, 2020

Abstract: Hardened layers are commonly required for automotive components after their production using a machining process in order to enhance the service life of these components. This study investigates the possibility of producing a nanostructured machined surface which can increase the hardness of the machined surface by varying the machining parameters under cryogenic conditions in end milling of AISI 4340. The end milling experiments were performed using multi-layered TiAlN- and AlCrN-coated carbide. Prior to the experiment, a finite element method (FEM) was used to simulate the cutting temperature generated and it had been found that at cutting speed of 200–300 m/min, feed rate of 0.15–0.3 mm/tooth, axial depth of cut of 0.3–0.5 mm, and radial depth of cut of 0.2–0.35 mm, the temperature generated can be sufficiently high to cause austenitic transformation. A field emission scanning electron microscope (FESEM) equipped with angle selective backscattered (AsB) detection analysis was used to investigate the microstructure and machined-affected layers of the machined surfaces. The crystallographic orientation/phase change and nano-hardness were analysed through X-ray diffraction (XRD) and a nano-hardness testing machine. The results showed that the cryogenic machining had significantly affected the surface integrity characteristics of the AISI 4340 alloy due to refined microstructure, favourable phase structure, and higher hardness near the surface layer. The results of this study may be useful in providing an insight into a potential technological shift from conventional surface case hardening processes to the present technique.

Keywords: AISI 4340, cryogenic machining, hardness, surface integrity, FESEM, XRD

1 Introduction

Hardened surface is directly related to surface integrity, which is a significant performance measure in assessing the machinability of materials. Surface integrity is defined as the inherent or enhanced condition of a machined surface or other surface generation operation [1]. Shokrani et al. [2] grouped surface integrity into three subgroups: (1) mechanical properties, which relate to residual stress, hardness, and depth of hardness; (2) metallurgical properties, which relate to phase transformation, heat-affected zone, decarburization, property variation, and alloy depletion; and (3) topological properties of a machined surface which relate to surface roughness, geometrical accuracy, and texture waviness generated on the surface and sub-surface of the machined work piece. During machining, high heat is generated in the machining zone. This will lead to dimensional inaccuracy of the workpiece and the tool is also subjected to a larger thermal load leading to high tool wear. One of the approaches which could reduce the high temperature at the machining zone is by the application of cryogenic cooling. This strategy improves machining performance, lowers the heat generated, improves chip breakability, and has benefits from sustainable and ecological perspectives [3].

* **Corresponding author: Jaharah A. Ghani,** Centre for Materials Engineering and Smart Manufacturing (MERCU), Department of Mechanical and Manufacturing Engineering, Faculty of Engineering and Built Environment, Universiti Kebangsaan Malaysia, 43600 Bangi, Selangor, Malaysia, e-mail: jaharahaghani@ukm.edu.my
Shalina Sheik Muhamad: Centre for Materials Engineering and Smart Manufacturing (MERCU), Department of Mechanical and Manufacturing Engineering, Faculty of Engineering and Built Environment, Universiti Kebangsaan Malaysia, 43600 Bangi, Selangor, Malaysia; Prototype and Plant Development Center (PDC), Department of Technical Support Division, Malaysian Nuclear Agency, 43000 Bangi, Selangor, Malaysia
Che Hassan Che Haron: Centre for Materials Engineering and Smart Manufacturing (MERCU), Department of Mechanical and Manufacturing Engineering, Faculty of Engineering and Built Environment, Universiti Kebangsaan Malaysia, 43600 Bangi, Selangor, Malaysia
Hafizal Yazid: Materials Technology Group (MTEG), Industrial Technology Division, Malaysian Nuclear Agency, 43000 Bangi, Selangor, Malaysia

There have been many studies related to cryogenic machining-induced surface integrity due to its competitive advantages. Many researchers have conducted studies on the benefits of cryogenic machining correlated with the functional performance and service life of machined components. An extensive review about cryogenic process focusing on processes such as machining, forming, grinding, and burnishing has been presented by ref. [4]. In the review, they elucidate the historic analysis of process mechanics and material performance comprising tribological and thermo-mechanical interactions, surface integrity, product quality, and performance in cryogenic manufacturing. A literature review focusing on cryogenic machining of nickel alloys is provided by ref. [5]. This comprehensive review concluded that cryogenic machining processes significantly affect not only the surface quality characteristics of nickel alloys, but also help in tool-life, tool wear, and residual stresses. In the review of state-of the-art of the use of cryogenic cooling, [2] they classified into two major categories, namely cryogenic processing and cryogenic machining. This systematic review concluded that cryogenic cooling has demonstrated significant improvements in machinability by changing the material properties of the cutting tool and/or workpiece material at the cutting zone, altering the coefficient of friction, and reducing the cutting temperature.

Bruschi et al. [6] revealed the formation of an ultrafine surface layer in the cryogenic machined surface of AZ31B Mg, four times and almost twice wider than the dry and wet cut samples. This has a significant effect in terms of increased nano-hardness and presence of compressive residual stresses for the cryogenic machined sample attributes for the enhanced resistance of corrosion. Moreover, it has been reported that the application of liquid nitrogen (LN_2) could reduce tool wear, lower the required cutting force, improve surface roughness, lessen deformation of microstructure changes at the sub-surface level, and eliminate contamination of the machined part [7,8]. Compared with dry machining, it was found that the cryogenic machined surface had higher hardness. Hardness changes at the machined surface occurred due to the formation of ultrafine white globular particles. Higher density and more homogeneous ultrafine white globular particles in cryogenically machined surfaces are associated with carbide precipitates, which substantially contributed to the higher hardness [9].

Zheng et al. [10] conducted a study of surface integrity in dry machining of AISI 4340 alloy. The surface integrity studies are focused on the surface roughness, microstructure, residual stress, and micro-hardness of the machined surface. They found that the grain refinement with slip, twin, or their combination is observed by using electron backscattered diffraction (EBSD) technique. As a result of the surface transformation and recrystallization, it had influences on the residual compressive stress and work hardening. They also reported that plastic deformation causes the variation range of the work hardening degree of 110–120%. The range of the hardening depth is about 60–80 μm. They also pointed out that within this range of work hardening degree, it is beneficial in terms of wear and corrosion resistance of the components and parts.

Several studies utilize the finite element method (FEM) in obtaining more understanding on the machinability of cryogenic application during the machining process. Caudill et al. [11] used DEFORM as a FEM tool for predicting cutting forces and temperature distributions during machining of Ti_6Al_4V for cryogenic and flood-cooled conditions. They revealed that the numerical predictions are in good agreement with the experimental observation. They also reported that 40% of the cutting temperature generated during machining was reduced by the application of the LN_2. To date, several studies have explored the use of FEM on surface integrity during cryogenic machining. Kim et al. [12] conducted an investigation of the effects of cryogenic cooling on the cutting force, microstructure, surface integrity, and burr height. The cutting temperature, cutting force, and chip morphology were simulated by the FEM model. The predicted forces showed good agreement with the experimental data, and the simulated chip shape matched well with the experimental data. Shen et al. [13] investigated the different tool edge radii on predicting grain size, micro-hardness, and residual stress using a physics-based material model for magnesium alloy. These studies indicate that applying cryogenic cooling or a larger edge radius could increase the surface hardness. The micro-hardness was increased as high as 0.4 GPa (75%) on both machined surface and tool–chip interface of cryogenic machining with 70 μm edge radius. FE model has been able to predict the slip/twinning transition and twinning lamellas at the topmost surface layer. The simulated grain sizes were about 62–64 nm on top of the ultrafine layer as thick as 18 μm of cryogenic machining with 70 μm edge radius. Overall, these FEM studies provide strong evidence that a good agreement was observed between the simulated and experimental results.

Thermo-mechanical effects on the machined surface during machining exhibited different microstructure from the bulk workpiece material. This layer is called the machining-affected layer. Depth of the machining-affected layer, variation of grain size, and grain orientation through recrystallization and recovery, in addition to phase transformation,

were the common parameters which characterized the microstructure alterations induced by machining processes [14]. During machining, there are two main layers generated in the surface region [15]. The layers are the refined grain layer (RL) and the transition layer (TL). The properties of these layers differ from the bulk in terms of mechanical properties and chemical composition. Thickness of the layers depends on the work material properties, cutting conditions, and cutting parameters. During cryogenic machining, the refined layer is formed with the increase in surface hardness and compressive residual stress.

The concept of phase transformation is complex, since it involves several interdependent interactions. Mechanical deformation, heat transfer, and phase transformation are related to each other in the cutting process of steel. The metallo-thermo-mechanical coupling has been used to describe this relationship. Temperature affects the stress/strain and phase transformation. Phase transformation consequently affects stress/strain by causing transformation strain. The reverse effect, which is strain-induced transformations, can also probably occur. Strain also alters the temperature due to mechanical work which is plastic deformation and friction. Latent heat from phase transformation also alters the thermal field. Large strains can also assist in phase transformations, named as strain-induced transformation. Lastly, chemical concentrations, such as carbon content in steel, will have an effect on and can be affected by all three fields [16,17].

The Hall–Petch equation was used in the nano-hardness to show the role of grain boundary strengthening [18]. The relation between grain size and hardness has been shown in equation (1) below

$$\sigma = \sigma_0 + kd^{-1/2} \tag{1}$$

where σ is the yield stress, σ_0 is the intrinsic strength of the metal, k is a coefficient, and d is a grain diameter or the size of the grain. The Hall–Petch equation shows that reducing the grain size leads to an increase in the stress concentration at the grain boundaries which results in increased strengthening compared with coarse-grained materials [19]. Pu et al. [20] reported that cryogenic machining reduced the grain size of AZ31B Mg alloy from 12 µm to 31 nm and remarkably improved its functional performance, including hardness, corrosion/wear resistance, and fatigue life. Branco et al. [21] mentioned the presence of annealed martensite at the machined surface generated by the thermo-mechanical effect. The phase transformation or the retempering of the welded martensite of the part was dependent on the machining parameters and was due to the rapid heating and cooling caused after the machining.

This paper presents experimental works of milling AISI 4340 using PVD-coated TiAlN and AlCrN carbide tool using various machining parameters. Two aspects of surface integrity were investigated, namely, the mechanical aspect, the metallurgy of the machined surface and sub-surface which includes machined surface alteration, phase transformation, and nano-hardness generated. The hardness results have been compared with those obtained by conventional surface case hardening. The main aim of this study is to explore the potential of utilizing LN2 in the machining process in order to eliminate the heat treatment process.

2 Methodology

2.1 FEM of orthogonal cutting of AISI 4340

In this study, temperature simulations of end milling were performed using commercial FEM software in the form of Third Wave AdvantEdge (v6.4) in two dimensional (2D) orthogonal cutting. AdvantEdge uses a Lagrangian mathematical formulation and dynamic code which can perform coupled thermo-mechanical transient analysis [22]. The input parameters defined included cutting speed, feed rate, axial depth of cut, radial depth of cut, work piece material, the initial temperature of the workpiece, cutting tool material, and geometries. These input parameters have been shown in Table 1. The Tecplot software allows users to display and analyse simulation results. The material of the workpiece, material of the tool, and tools coatings were chosen from the AdvantEdge material library.

AISI 4340 M (modified) and standard cemented carbide grade-P were chosen as the workpiece material and the cutting tool, respectively. This material was chosen

Table 1: Input parameters for FEM study

Cutting conditions	
Cutting speed, V_c (m/min)	200, 250, 300
Feed rate, f_z (mm/tooth)	0.15, 0.20, 0.30
Axial depth of cut, a_p (mm)	0.3, 0.4, 0.5
Radial depth of cut, a_e (mm)	0.20, 0.35, 0.50
Workpiece material	AISI 4340
Initial temperature	20°C
Cutting tool material	TiAlN/AlCrN
Tool diameter	20 mm
Rake angle	28°
Clearance angle	11°

because it has the closest chemical composition to the workpiece used in the experimental test. The hardness of the workpiece material was set to 300 BHN. The cutting tool coating thickness was set as one layer which was a 0.003 mm TiAlN coating. The carbide grade, the coating material, and layer thickness were chosen and set to be as close as possible to the real carbide insert used in the experimental test. The tool was defined as a rigid body which accounted for thermal transfer for modelling the cutting temperature field. The maximum and minimum element sizes for both workpiece and insert were set at 0.1 mm and 0.02 mm, respectively. The mesh refinement factor was set at the value of 2 and its coarsening factor was set to 6. The coolant temperature was set to –196°C, while the heat transfer coefficient, h, was set to 20,000 $W/m^2 K$, according to literature [23].

Table 3: Properties of LN_2 [25]

Density (kg/m^3)	807.3
Dynamic viscosity (mPa s)	0.158
Thermal conductivity (W/m K)	0.1396
Specific heat (J/kg K)	2,050
Boiling point (°C)	–196

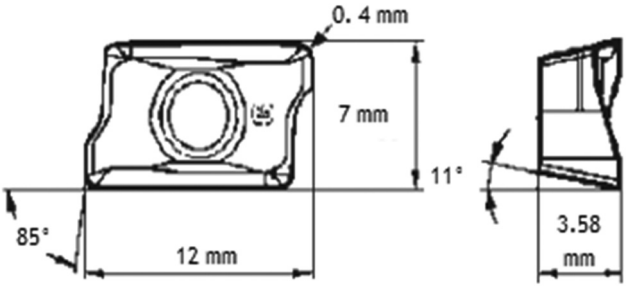

Figure 1: Schematic diagram and geometry of the cutting tool used in the experiment.

2.2 Machining experiment

The experiments were performed on a DMG-ECO, the three-axis vertical milling centre with a maximum spindle speed of up to 8,000 RPM. Machining was carried out by varying the parameters of cutting speed, feed rate, radial depth of cut, and axial depth of cut. The experimental conditions are shown in Table 2. The range of parameter set-up was based on the machine's capability, manufacturer's tools, and studies from previous research by Natasha et al. [24] and from the FEM simulation study for cutting temperature. The FEM simulation study found that the cutting temperature may reach above 700°C within this range of machining parameters, which will cause the phase transformation from austenite to martensite of AISI 4340.

The coolant used for cryogenic machining was LN_2 which was directly supplied to the cutting zone during the cutting process via a nozzle. The properties of LN_2 have been listed in Table 3. LN_2 was under 2 MPa pressure and with spray angle: 45°, spray distance: 50 mm, and approximately 1.159×10^{-3} m^3/s flow rate which had been set to ensure that there was no excessive cooling.

The cutting tool used in the experiments was a commercially available P ISO grade PVD multi-coated cemented carbide end mill insert with detailed geometry as shown in Figure 1. The coating was multi-layers of 3 µm coating thickness with alternating layers of TiAlN and AlCrN. A fresh cutting tool was used for each machining run to eliminate the influence of tool wear on the integrity of the machined surface. The workpiece material used was commercially available AISI 4340 steel with dimension of 165 mm × 100 mm × 100 mm. The hardness of the experimental materials was 32 HRC. The workpiece was machined along its surface of 165 mm, and the sample was cut at the middle for further sub-surface characterization and analysis. Table 4 shows the chemical composition of AISI 4340 steel. The mechanical and thermal properties of AISI 4340 steel are shown in Table 5.

This material is widely used in power transmission gears and shafts, couplings, aircraft landing gear, and the

Table 2: Experimental conditions for the machining test

Exp. no./sample no.	Cutting speed, v_c (m/min)	Feed rate, f_z (mm/tooth)	Axial depth of cut, a_p (mm)	Radial depth of cut, a_e (mm)
1	200	0.15	0.3	0.20
2	250	0.15	0.5	0.35
3	250	0.30	0.4	0.20
4	300	0.30	0.3	0.35

other structural parts which require strict geometric tolerance, superior surface quality, and longer service life [26]. The AISI 4340 is a commercial medium carbon low alloy steel which is categorized as hard to cut material due to the high hardness, high plasticity, inferior thermal conductivity, and high toughness [27,28]. The alloying element of AISI 4340 provides a good balance of strength, wear resistance, and toughness properties which make it outpoint than the normal steel. Therefore, it is important to explore the cryogenic environment and machining parameters of high-strength steel for achieving the highly efficient machining.

2.3 Sub-surface characterization

Metallography samples for sub-surface characterization were prepared by cutting them from the workpiece using the EDM process. The sizes of these samples were 5 mm × 5 mm × 5 mm. The samples were then mounted into a cold-setting epoxy. The prepared samples were ground and polished using a semi-automatic polishing unit. The rough grounding was performed on wet metallographic grinding paper of grit 240, followed by 400, 800, and finished with 1,200. The polishing was carried out using a Buehler Universal Polisher with 6 µm, followed by 1 µm polycrystalline diamond suspension to obtain a mirror-like surface. The samples were etched using 2% Nital solution for 10–15 s.

The sub-surface microstructure and machined-affected layers were observed by using a MERLIN Compact Zeiss FESEM equipped with an AsB detection. The composition and distribution of elements on the surface of the sample were observed using an Energy Dispersive X-Ray Analysis (EDX) microanalysis system.

XRD studies were performed to investigate the microstructural phase composition of the machined surface with XPERT-PRO X-ray diffractometer (XRD). The XRD patterns were measured using Cu Kα radiation from a source operated at 40 kV and 30 mA. The 2θ scans were carried out between 5.0167° and 79.9597° where the scan increment was 0.0330° and the scan step time was 39.5120 s. After X-ray scanning of the samples, based on the peak positions and intensities, the peak positions were identified by the use of EVA software.

The nano-hardness of the surface and sub-surface was estimated by making indentations using a nano-hardness testing machine along the cross-section of the polish samples. Indentations of sub-micron depth were made by using a Berkovich indenter (three-faced diamond pyramid) on a nano-hardness tester (NTX NanoTest, made by Micro materials). The indenter load was set at 70 mN and loading rate of 4.5 mN/s was applied from 10 to 130 µm from the surface layer. The measurement was performed at every 20 µm from near the surface layer towards the centre of the specimen. Eighty four indentations were made in the form of a rectangular array. Three indentations were made at three different spots at each level of depth. The average of the hardness was taken by discarding the values which were considerably outside the range.

Table 5: Mechanical and thermal properties of hardened AISI 4340 steel [29]

Property	AISI 4340 steel	
	35 HRC	45 HRC
Density (kg/m^3)	7,830	7,850
Specific heat (J/kg K)	519	475
Thermal conductivity (W/m K)	42.3	44.5

3 Results and discussion

The results of cutting temperature, measured depth of the affected layers, and nano-hardness after machining at various machining parameters have been shown in Table 6. The simulated temperature field of the machined surface reached 850.8°C for experiment no. 4, which was high enough to induce martensite phase transformation.

Figure 2 shows the simulated temperature contour for sample no. 4 with the maximum surface temperature of 850.8°C. As shown in Figure 2, the highest temperature was at the tool–chip interface. The results discussed in

Table 4: Chemical compositions of AISI 4340 [19]

Element	C	Si	Mn	P	S	Cr	Mo	Ni
Minimum (%)	0.37	0.10	0.55	0	0	0.65	0.20	1.55
Maximum (%)	0.44	0.35	0.90	0.04	0.04	0.95	0.35	2.00

Table 6: FEM simulation data for predicted cutting temperature, measured depth of the affected layers, nano-hardness, and surface roughness after machining at various machining parameters

Exp. no./ sample no.	Temperature (°C)	RL (μm)	TL (μm)	Affected layers RL + TL (μm)	Nano-hardness (GPa)	Surface roughness (μm)
1	576.2	4.34	18.78	23.12	3.11	0.114
2	731.6	5.24	25.22	30.46	3.59	0.166
3	716.9	7.12	32.37	39.49	4.10	0.227
4	850.8	7.48	28.90	36.38	4.73	0.184

Natasha et al. [30] revealed that the highest temperature always occurs at the secondary deformation zone, which is around the middle tool–chip contact area on the rake face.

The original microstructure of AISI 4340, i.e., before machining process has been shown in Figure 3 and Figure 4, showing the FESEM images of the machined surface, revealed the apparent plastic deformation beneath the surface. The microstructure in Figure 5 is obviously a different microstructure from the bulk material as observed in Figure 4. The bulk grain structure on the as-received sample had a clear grain boundary, but these were not observed as the microstructure becomes dense in Figure 5. The grains in the machined surface samples had been stretched and crushed due to the mechanical deformation during the machining process. Moreover, the structure also showed that the white carbide particles were distributed in the grain structure. Figure 5 shows the cross-sectional view of the sub-surface microstructure at 1,000× magnification. The depth of microstructure alteration beneath the machined surface has been measured from the top region for each of the machined surface samples. The thickness of the RL and the TL produced after machining under cryogenic environment at various machining parameters have been shown in Figure 5 and Table 6.

Figure 5 confirmed that the nanoscale grains at the top region went down several micrometres beneath the machined surface. Zones showing the surface layer having different microstructure and grain refinement zones have been clearly shown. These zones resulted from rapid heating and quenching, leading to untempered martensitic structures [31]. The effect of grain size on the mechanical properties is mainly reflected in the microstructure [32–34]. The grains in the alloys can be greatly refined under high strain and strain rate [35]. The strain in the refined layer is larger than that in the bulk material, as shown in Table 7, so it can indicate that the refined layer is subjected to severe plastic deformation. Severe plastic deformation can also speed up the process of grain refinement [36]. Plastic deformation also stimulates the movement of lattice dislocations [37].

From Figure 5, the affected depth on the sub-surface was dependent on the cutting parameters. The increase of cutting conditions from low to high level produced

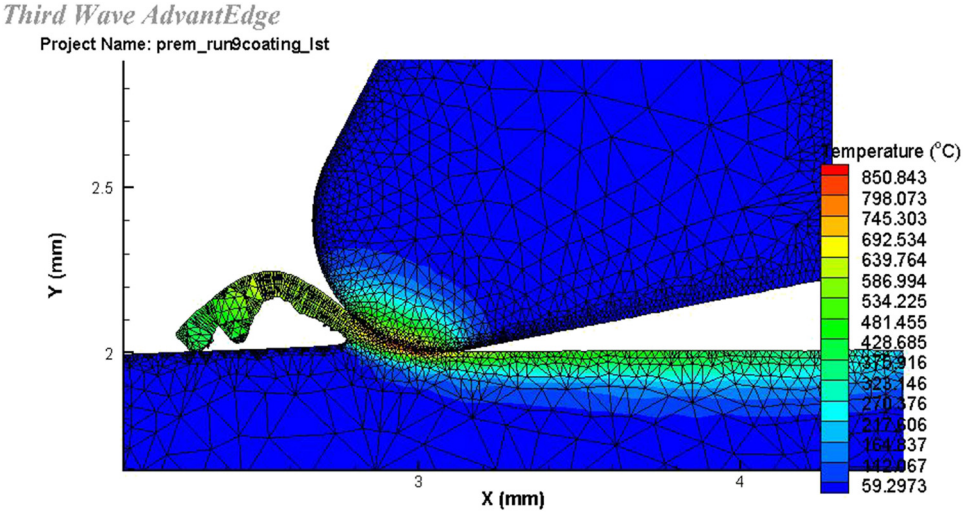

Figure 2: Simulated temperature field for sample no. 4.

relatively deeper alteration of the microstructure. The increase in affected depth may have been due to the increasing area in the sub-surface where the temperature exceeded the austenitization temperature for subsequent quenching through self-cooling. The higher temperature rise around the edge tip also resulted in localization of thermal softening in the workpiece material [38].

From Table 6, the deepest affected depth obtained was 39.49 µm at a speed of 250 m/min, feed rate of 0.3 mm/tooth, axial depth of cut of 0.4 mm, and radial depth of cut of 0.2 mm. The thickness of affected depth when machined at 0.4 mm axial depth of cut was higher than that when machined at 0.3 mm. This may have been due to the higher cutting forces generated to remove the unwanted material. Meanwhile, the lowest affected depth obtained was 23.12 µm at a speed of 200 m/min, feed rate of 0.15 mm/tooth, axial depth of cut of 0.3 mm, and radial depth of cut of 0.2 mm. The depth of affected layer was also dependent on the temperature where the less severe parameters had the lowest temperature, thus the dislocation became much harder and consequently the depth of the affected layer became smaller. This observation was consistent with the nano-hardness measured. This observation was in line with previous findings by other researchers who claimed that the microstructure alteration of machining-affected layer causes it to be harder than the bulk hardness of the workpiece after machining [14,39].

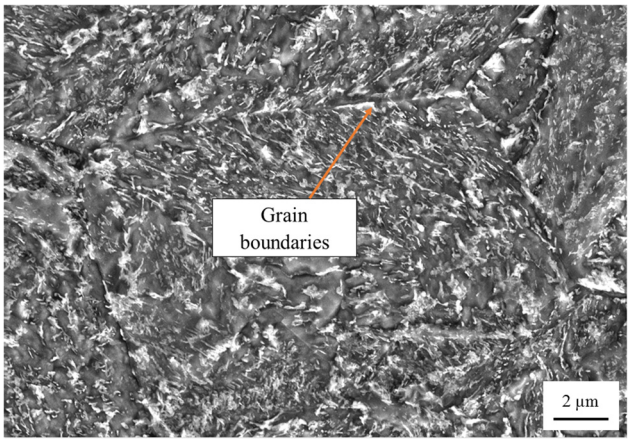

Figure 3: Microstructure of the bulk material of AISI 4340.

X-ray line scanning and mapping was carried out to determine the chemical composition and carbides particles in the metal matrix. Figure 6 shows all elements in the surface machine-affected layer for Sample 4. It could be seen that there was a difference in chemical composition of the layer, compared with the bulk material. EDX analysis on the machine-affected layer showed that there was higher carbon content compared to the as-received sample. Increase in carbon content results in high strength of steel and produces large amounts of carbide particles. The increase of carbon on the machined surface may be due to the presence of retained austenite and diffusion of carbon to the workpiece [40]. The carbon steel can undergo high-temperature tempering when the temperature exceeds 500°C. After high-temperature tempering, martensite is decomposed into ferrite and precipitation of carbide [41]. Umbrello et al. [42] verified a carbon content in the surface layer of AISI 52100 steel samples after machining under dry and cryogenic conditions in comparison with the unmachined sample. They observed the presence of an increase in carbon compared to the unmachined sample and this was consistent with surface hardness modification. This showed that chemical composition plays an important role in increasing surface hardness.

The effect of different machining conditions on phase transformation of the AISI 4340 alloy was studied. Figure 7 shows the phase analysis obtained by XRD technique on

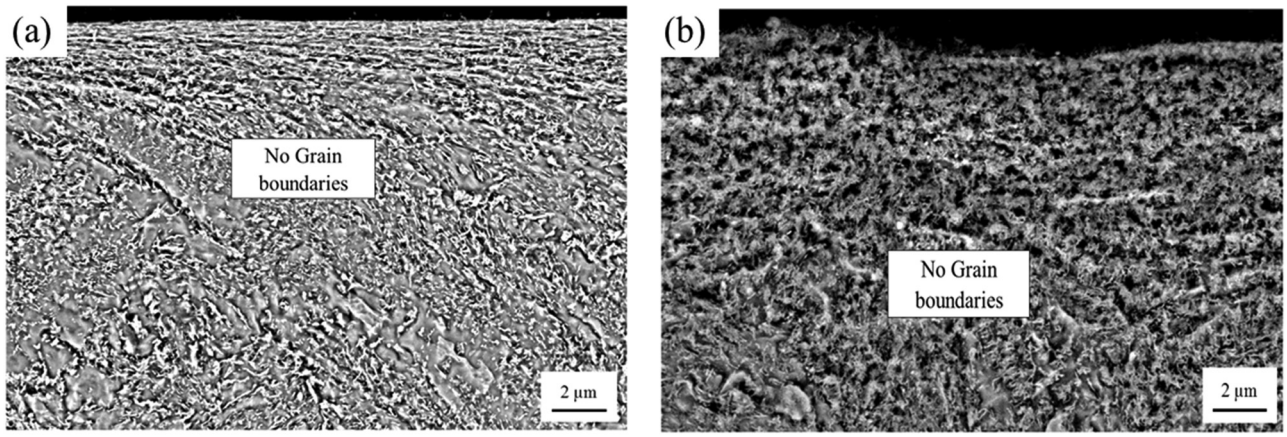

Figure 4: Microstructure beneath the machined surface of sample no.: (a) 2 and (b) 4.

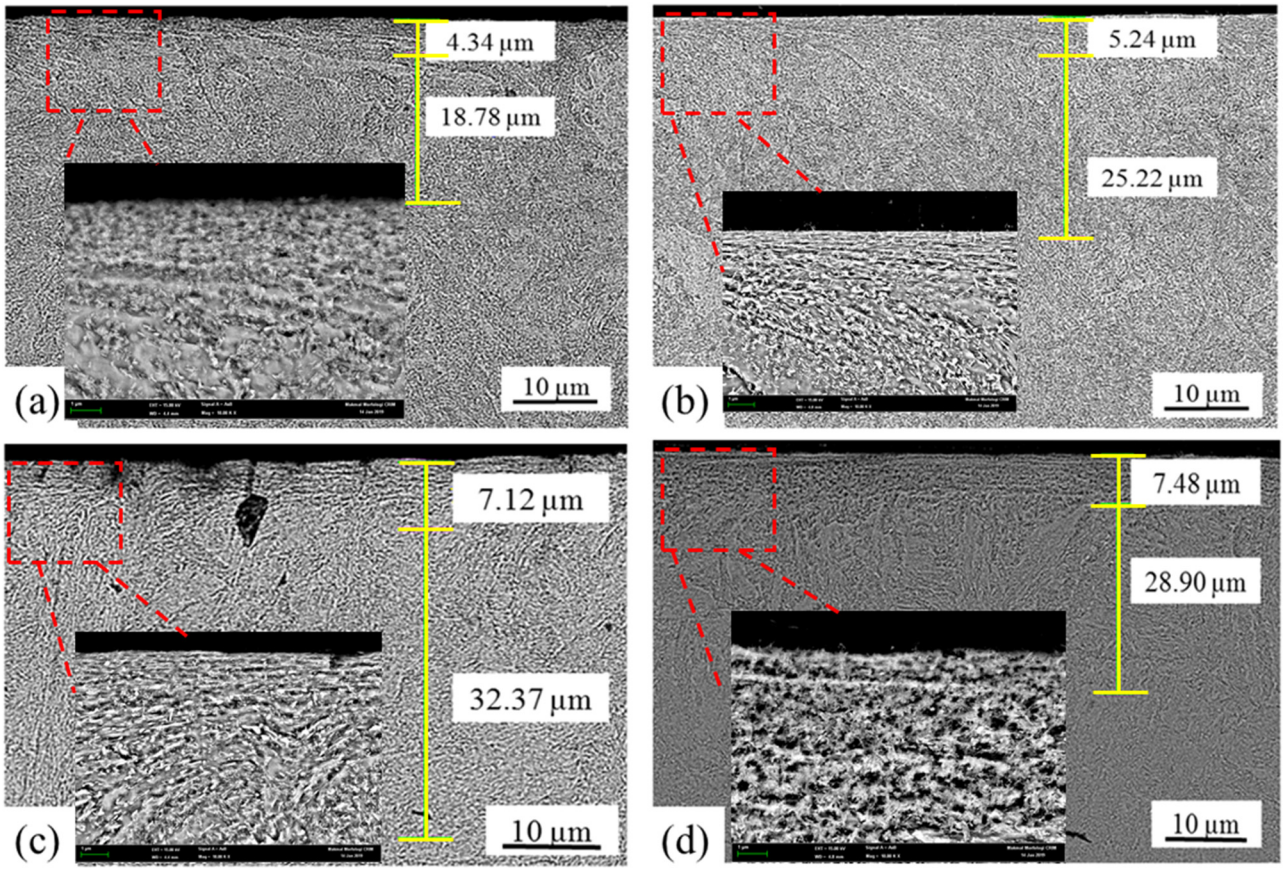

Figure 5: Microstructure beneath the machined surface and machining-affected layer of sample no.: (a) 1, (b) 2, (c) 3, and (d) 4.

Table 7: Crystallite size and lattice strain of the XRD spectra at various machining parameters

Exp. no./sample no.	Crystallite size (Å)	Lattice strain (%)
As-received	405	0.226
1	377	0.242
2	361	0.254
3	388	0.237
4	331	0.278

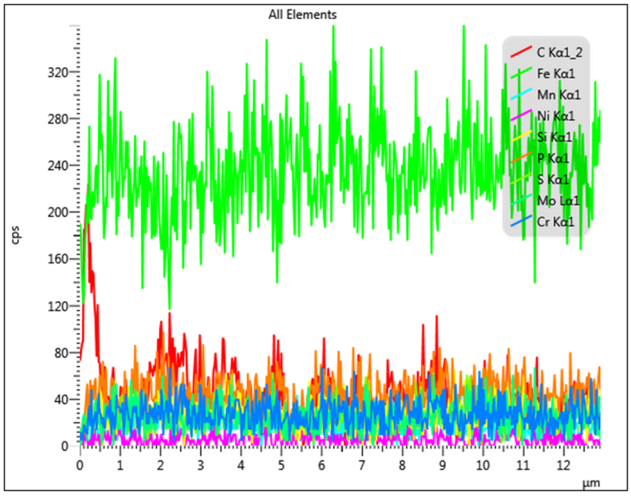

Figure 6: FESEM-EDX line scanning analysis along the thickness of the 0–13 µm in sample 4.

as-received and machined samples under various machined conditions. X-ray phase analysis on the as-received surface and on machined sample showed two peaks at 44.6° and 65° at 2θ values. X-ray phase analysis conducted on machined samples showed that the peaks had a lower relative intensity compared to the as-received samples. The same pattern had also been obtained by other researchers [9,43].

Figure 7 shows the X-ray spectra of the samples before and after machining at the various planes of (110), (101), and (200). According to the PDF2-2004 cards, the peaks of ferrite-α at (110) Miller indices were found for the as-received Samples 1 and 2. The peaks of martensite at (101) Miller indices were found for Samples 3 and 4. Diffraction analysis on the samples after machining revealed that there were phase changes in Samples 3 and 4 as

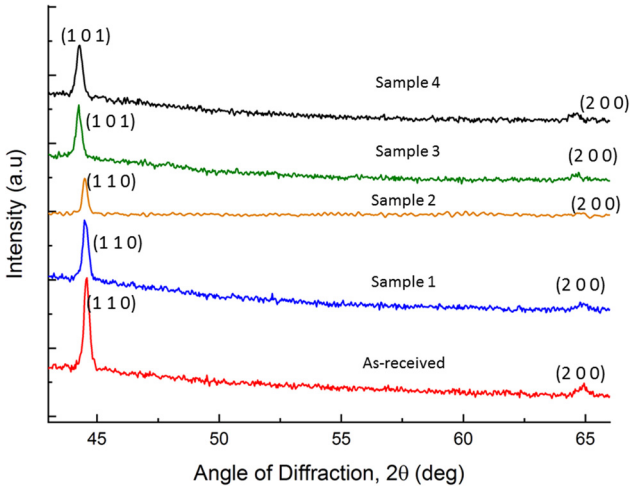

Figure 7: XRD phase analysis of the as-received and machined surface under various cutting conditions.

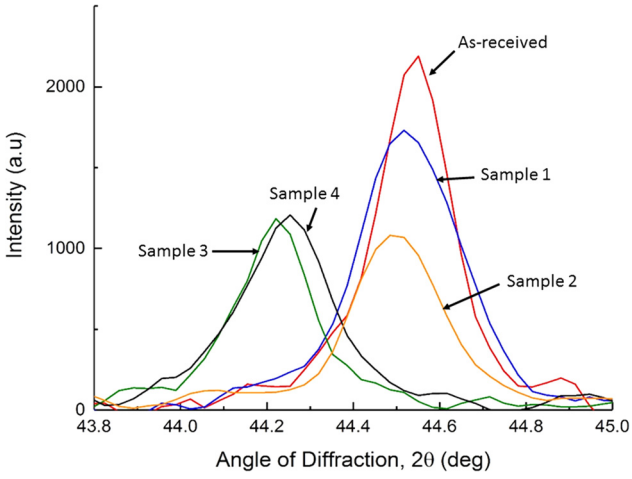

Figure 8: XRD spectra at the various reflecting planes of the as-received and machined surface under various cutting conditions.

obtained by Kim and Kwon [44]. From the above results, it can be stated that the high machining temperature and the faster cooling rate due to the application of LN_2 promoted the phase transformation.

All machined surfaces showed the broadening of the peak width as well as the peak shifting to a lower angle compared to the as-received material as illustrated in Figure 8. The finding was consistent with the findings of past studies by Kaynak et al. [45] that cryogenic machining generates broadening peaks. The broadening of the peaks is due to the plastic deformation and formation of dislocations density produced by cutting processes caused by micro strain and crystal lattice distortions [46,47]. Lattice strain is a measure of the distribution of lattice dislocations, which arise from crystal imperfections [48]. The broadening peak under high level cutting condition compared with low level cutting condition could have been caused by more severe work hardening and/or smaller grain size. The hardness of the samples as shown by Figure 9 correlated well with the broadening of curves, which shows that the hardness and work hardening are intimately related [49]. Sun et al. [50] observed that the higher strain causes higher dislocation density and helps in dislocation movement, which can enhance the grain refinement.

According to literature, the transformation temperature of this material is approximately 800°C [51]. The phase transformation model also could be obtained from the time–temperature–transformation (TTT) curve [52]. Based on the TTT curve as the workpiece begins to cool, austenite transforms to martensite if the cooling rate is fast or to bainite if the cooling rate is slower. However, this temperature is not considering the stress-strain effects which were generated during the machining. If the workpiece temperature exceeds the phase transformation temperature, an austenitic transformation occurs which is an indicator of phase transformation. However, the phase changes can start at a lower temperature of nominal phase change temperature due to high stresses and strains induced by machining [51].

Regarding the phase transformation mechanism, it is known that the temperature at the tool/workpiece interface can reach high enough to cause a phase transformation. If the heat flux is high enough to reach the phase transformation temperature, then by rapid cooling, the austenite is partly transformed into martensite and

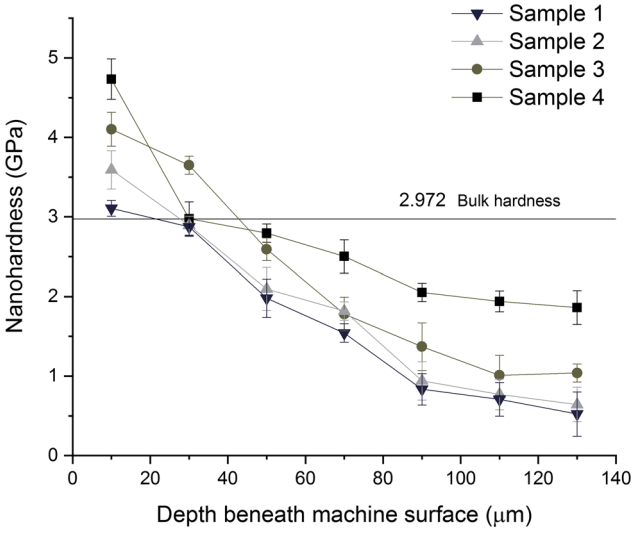

Figure 9: The nano-hardness value measured on the sub-surface of the machined surface under various cutting conditions.

retained austenite remains [53]. During the machining process, the surface temperature increases significantly and the rapid cooling by LN_2 simulates the quenching effects. Rapid quenching is a major part in the hardening mechanism of the steel hardening by heat treatment [54]. The phase transformation is affected by strain, strain rate, and temperature, the three important processing parameters in any mechanical process [55].

The relationship between lattice strain and crystallite size was estimated by X'Pert HighScore Plus software based on XRD patterns. The Scherrer equation (equation (2)) is used to calculate the lattice strain and crystallite size. The peak width, β in radians, measured as full width half-maximum of an X-ray diffraction (XRD) spectra, is inversely proportional to the crystallite size L_{hkl} perpendicular to the *hkl* plane [19,56]:

$$L_{hkl} = \frac{\lambda}{(\beta \cos \theta)} \tag{2}$$

Table 7 shows that lattice strain increases and crystallite sizes decrease with the increasing of machining parameters. The average crystallite sizes in the machining-affected layer are smaller than bulk regions which is consistent with the microstructure observed in the backscattered electron images shown in Figure 5. The crystallite size becomes smaller when the cutting condition is more severe. As shown in Table 7, crystallites up to about 331 Å in size were formed on the sub-surface of the machined surface. The lattice strain of sample no. 4 is as high as 0.278%, which is much higher than sample no. 1. The dislocations are more as the strain increases; as can be seen in Figure 8, the sample no. 4 showed the more broadening of the peak width compared to the other samples. As a consequence of dislocation, new dislocation boundaries are formed which can subdivide the original grains into subgrains [57]. Based on Table 7, the crystallite size was reduced maximum up to 18.3% as compared to the as-received sample.

It shows that cryogenic machining enables generation of smaller crystallite size in the sub-surface of the machined sample. This, according to the Hall–Petch equation (equation (1)), demonstrated that the machine samples with smaller average crystallite sizes have higher strength (hardness) than the as-received samples, which was confirmed by the hardness of the former samples. The results of this investigation show that the machine-affected layer is induced by the interaction of phase transformation and plastic deformation. The fine crystal sizes and high strains are due to plastic deformation which occurs during machining, as reported by Duan et al. [43].

The nano-hardness variation from the machined surface towards the centre of the samples under different cutting parameters has been shown in Figure 9. In this study, all samples tested showed the increment of the hardness at the surface and sub-surface of the machined part. The point closest to the machined surface was found to have higher hardness than the initial material hardness. After the highest hardness had been reached, the average hardness gradually decreased until achieving the bulk hardness at about 22–42 µm beneath the machined surface. Then, it started to stabilize at around 90 µm from the machined surface. Figure 9 shows that the variations of the sub-surface nano-hardness depend only on the cutting parameters and cryogenic cooling because the samples had been prepared with the use of a sharp tool. The results not only have the same trend, but also at 20–40 µm beneath the machined surface, the nano-hardness value was lower than that of the bulk material. This indicated that the affected layers were relevantly related to the additional tempering in machining and resulted in a lower hardness. A tempering effect was generated because the temperature was not high enough at this distance from the surface for phase transformation of the material and the cooling time was longer [58]. These results were consistent with the fact that the region was most likely composed of over-tempered martensite [58–60].

The hardness increased 59% from 2.97 GPa in the bulk material to 4.71 GPa after machining at a speed of 300 m/min, feed rate at 0.3 mm/tooth, axial depth of cut at 0.3 mm, and radial depth of cut at 0.35 mm. Meanwhile, the lowest hardness obtained was at a speed of 200 m/min, feed rate at 0.15 mm/tooth, axial depth of cut at 0.3 mm, and radial depth of cut at 0.2 mm. It only increased in nano-hardness by approximately 4.71% more than the bulk hardness. From the above results, it can be stated that the cutting parameters play an important role in the value of nano-hardness. It could also be due to the time contact as at the lower machining parameters, the workpiece material cooled faster, thus reducing the effect of work hardening. The results showed that the higher the cutting speed and feed rate, the higher the surface nano-hardness and also the thicker the affected layer. The hardness improvement could be attributed to the transformation of an amount of the austenite to martensite as mentioned above.

Temperature and time are the main factors in the machining hardening mechanism. The depth of hardened layer could be increased if the heat flux into the workpiece is high and contact time is sufficiently long to penetrate high-temperature contours (over austenitizing temperature). Contact time is VB/v, where VB is tool

wear land and v is the cutting speed [61]. A numerical prediction model using PCBN tool hard cutting hardened steel $Cr_{12}MoV$ showed that the closer the temperature surface layer is to the machined surface, the denser the temperature gradient is ref. [62]. A comprehensive study of the effects of cutting parameters (depth of cut, feed rate, and cutting speed) on the hardening showed that feed rate has the greatest effect on hardness as feed rate generates higher cutting forces and therefore more plastic deformation. Surface hardness increases with increment of depth of cut as it influences the tangential cutting force. The hardness also increases with cutting speed. This is because the increasing speed generates a higher strain rate, which leads to compressive stresses due to additional work introduced to the process [63].

Strain hardening and grain refinement may be the other contributing factors to the increases in the hardness on the surface and sub-surface of the cryogenic machined parts [13]. From the Zenner–Holloman equations, there is a relation between grain size, strain rate, and temperature as shown in equation (3)

$$\frac{d_{\text{rec}}}{d_{\text{initial}}} = 10^3 \times Z^{-1/3} = 10^3 \left[\dot{\varepsilon} \exp\left(\frac{Q}{RT}\right) \right]^{-1/3} \tag{3}$$

where d_{initial} is the initial grain size of the work material, d_{rec} is the recrystallized grain size after the deformation process, $\dot{\varepsilon}$ is strain rate, and T is temperature. Z, R, and Q are material constants. The Zener–Hollomon equation shows that the two main factors affecting grain refinement are strain rate and temperature. In this case, cryogenic machining could alter the cutting temperature field. The heating–cooling cycle in cryogenic machining which depicted the quenching process also contributes some important aspects to the hardening mechanism [64]. Therefore, the hardness alteration would be a combination of factors, such as machining parameters, contact time, microstructure, and work hardening. It has been reported by other researchers [63,65] that the superficial hardening occurs due to many reasons, which are due to the microstructural changes, plastic deformation, and residual stresses introduced into the material.

As concerns the grain size trend, the grain refinement is increasing with the cutting speed, which is due to a larger Zener–Hollomon parameter as a consequence of higher strain rate and higher temperature near to the shear zones. These results are in agreement with Imbrogno et al.'s [66] findings that higher the cutting speed, higher grain refinement was expected due to the strain rate on the workpiece due to the tool action. It is possible that higher hardness was due to the grain refinement and the precipitation strengthening present. These results can be assuredly ascribed to the fact that experimental studies of the surface hardness were carried out in combination with the prediction of the new crystallite size.

In this study, the depth of the affected layer is comparable to the shallow case depth from the surface hardening processes. This can be as low as less than 0.25 µm during ion implantation where the case depths are shallow [67]. The minimum case depth which has been obtained by ion nitride of AISI 4340 steel at temperature of 500°C and nitriding time of 2 h is 280 µm [68,69]. The investigation by Chou [61] of AISI 4340 steel bars machined at 1.2 mm flank wear (VB) showed the hardened depth is about 30 µm. The hardness increases to maximum 49 HRC from 28 HRC of the bulk hardness. Also, Hassanpour et al. [40] reported that the hardness value increased from 450 HV to 607 HV for a hard milling of 4340 alloy steel using minimum quantity lubricant. The time required for machining is far shorter than that for conventional hardening. Furthermore, the surface roughness obtained was between 0.114–0.227 µm, which was similarly obtained with manual grinding [70] and no further polishing was required to obtain mirror-like surface. One of the strengths of this study is the remarkable result in surface roughness compared with the earlier findings reported by Natasha et al. [24].

The enhancement of mechanical properties of the final surface of the components was widely studied in various areas and surface modification is very important. Maochuan et al. [71] studied the effect of surface modification of nano-sized carbon black on reinforcement of rubber and found that surface activity, iodine adsorption number, and nitrogen surface area values of carbon black nanoparticles increased with the increase of temperature. Coating strategies for atomic layer deposition (ALD) were discussed by Hu et al. [72] focusing on coating strategies in ALD, emphasizing the recent progress in the fabrication of novel nanostructures. In medical applications, Ali et al. [73] studied the zinc-based nanoparticles (NPs) which can increase the particle surface reactivity and exhibit attractive antimicrobial and photocatalytic properties due to the smaller particle size, which are more biocompatible compared to other metallic NPs.

4 Conclusions

The conclusions of this study have been summarized below:

1. The temperature in the cutting zone was obtained by the FEM. It was found that the simulation result ranged from

576.2°C to 850.8°C. The predicted values exceeded the austenitizing temperature for AISI 4340 which is approximately 800°C.

2. Machine-affected layer on the surface of the machined samples ranged from 23.12 µm up to 39.49 µm. Microstructural changes with grain refinement in the surface layer were observed, with nanocrystalline structures with grain sizes in the range of 331–388 Å present in the machined samples. The thickness of the machine-affected layer with grain refinement was also found to be dependent on the machining parameters and the cutting temperature.
3. The XRD results showed that the machined AISI 4340 steel consisted of ferrite-α and martensite due to the rapid cooling of the surface, which should significantly enhance the hardness of the AISI 4340 steel.
4. EDX analysis showed that at higher cutting parameter *C*, weight percent was also increased. As a result, the increase in carbide particles can improve the hardness by changing the chemical composition of the materials.
5. The largest hardness increase of 59% was observed on the sample with the thickest grain RL in the machined surface layer after cryogenic machining compared to bulk hardness.

The experimental results from this study revealed a huge potential to use cryogenic cooling with appropriate machining parameters to improve the machined hardness. The cryogenic machining hardening method has an excellent economical and high sustainable manufacturing process due to its competitive advantages. Heat treatment can be eliminated and product cycle time can be reduced significantly. Cutting fluids are not required in this machining approach. LN_2 dissipates to the atmosphere, thus there is no air pollution and no after-treatment is required.

Acknowledgments: This work was supported by the Government of Malaysia and Universiti Kebangsaan Malaysia [grant numbers DIP-2018-048, GUP-2017-048] and FRGS/1/2016/TK03/UKM/01/1. The authors gratefully thank the MERCU, CRIM, and IMEN at the Universiti Kebangsaan Malaysia for their support for this research work. The authors also would like to acknowledge MTEG at Malaysian Nuclear Agency for their help with experimental work and analysis of results.

Conflict of interest: The authors declare no conflict of interest regarding the publication of this paper.

References

[1] Astakhov VP. Surface integrity–definition and importance in functional performance. Surface Integrity in Machining. London: Springer-Verlag; 2010. p. 1–35.
[2] Shokrani A, Dhokia V, Muñoz-Escalona P, Newman ST. State-of-the-art cryogenic machining and processing. Int J Comput Integr Manuf. 2013;26(7):616–48.
[3] Muhamad SS, Ghani JA, Haron CHC. A review on future implementation of cryogenic machining in manufacturing industry. Prog Ind Ecol An Int J. 2018;12(3):260–83.
[4] Jawahir IS, Attia H, Biermann D, Duflou J, Klocke F, Meyer D, et al. Cryogenic Manufacturing Processes. CIRP Ann Manuf Technol. 2016;65:713–36.
[5] Deshpande YV, Andhare AB, Padole PM. How cryogenic techniques help in machining of nickel alloys? A review. Mach Sci Technol. 2018;22(4):543–84.
[6] Bruschi S, Bertolini R, Ghiotti A, Savio E, Guo W, Shivpuri R. Machining-induced surface transformations of magnesium alloys to enhance corrosion resistance in human-like environment. CIRP Ann. 2018;67(1):579–82.
[7] Muhamad SS, Ghani JA, Juri A, Haron Che HC. Dry and cryogenic milling of AISI 4340 alloy steel. J Tribol. 2019;21:1–12.
[8] Musfirah AH, Ghani JA, Che Haron CH. Tool wear and surface integrity of inconel 718 in dry and cryogenic coolant at high cutting speed. Wear. 2017;376–377:125–33.
[9] Raof NA, Ghani JA, Haron CHC. Machining-induced grain refinement of AISI 4340 alloy steel under dry and cryogenic conditions. J Mater Res Technol. 2019;8(5):4347–53.
[10] Zheng G, Cheng X, Dong Y, Liu H, Yu Y. Surface integrity evaluation of high-strength steel with a TiCN-NbC composite coated tool by dry milling. Meas J Int Meas Confed. 2020;166:108204.
[11] Caudill J, Schoop J, Jawahir IS. Numerical modeling of cutting forces and temperature distribution in high speed cryogenic and functional and flood-cooled milling of Ti–6Al–4V. Procedia CIRP. 2019;82:83–8.
[12] Kim DY, Kim DM, Park HW. Predictive cutting force modeling for cryogenic machining process considering micro-structural analysis of Ti–6Al–4V alloy. Int J Adv Manuf Technol. 2018;189–92.
[13] Shen N, Ding H, Pu Z, Jawahir IS, Jia T. Enhanced surface integrity from cryogenic machining of AZ31B Mg alloy: a physics-based analysis with microstructure prediction. ASME J. Manuf. Sci. Eng.. 2017;139(6):061012.
[14] Wang B, Liu Z. Influences of tool structure, tool material and tool wear on machined surface integrity during turning and milling of titanium and nickel alloys: a review. Int J Adv Manuf Technol. 2018;98(5–8):1925–75.
[15] Kaynak Y, Lu T, Jawahir IS. Cryogenic machining-induced surface integrity: a review and comparison with dry, MQL, and flood-cooled machining. Mach Sci Technol. 2014;18(2):149–98.
[16] Bailey NS, Tan W, Shin YC. Predictive modeling and experimental results for residual stresses in laser hardening of AISI 4140 steel by a high power diode laser. Surf Coat Technol. 2009;203(14):2003–12.

[17] Inoue T. Metallo-thermo-mechanics—application to quenching. Handbook of residual stress and deformation of steel. Ohio, USA: ASM International; 2002. p. 296–311.
[18] Orlova TS, Mavlyutov AM, Latynina TA, Ubyivovk EV, Schneider R, Gerthsen D, et al. Influence of severe plastic deformation on microstructure, strength and electrical conductivity of aged Al–0.4Zr(Wt%) alloy. Rev Adv Mater Sci. 2018;55(1):92–101.
[19] Boakye-Yiadom S, Bassim N. Effect of heat treatment on stability of impact-induced adiabatic shear bands in 4340 steel. Mater Sci Eng A. 2012;546:223–32.
[20] Pu Z, Outeiro JC, Batista AC, Dillon Jr OW, Puleo DA, Jawahir IS. Enhanced surface integrity of AZ31B Mg alloy by cryogenic machining towards improved functional performance of machined components. Int J Mach Tools Manuf. 2012;56:17–27.
[21] Branco FK, Delijaicov S, Bortolussi R. Surface integrity analisys in the hard turning of cemented steel AISI 4317. Mater Res. 2018;21(5):1–9.
[22] Markopoulos AP. Finite element method in machining processes. SpringerBriefs in Applied Sciences and Technology Manufacturing and Surface Engineering. London: Springer; 2013.
[23] Kheireddine AH, Ammouri A, Lu T, Dillon Jr OW, Hamade RF, Jawahir IS. An experimental and numerical study of the effect of cryogenic cooling on the surface integrity of drilled holes in AZ31B Mg alloy. Int J Adv Manuf Technol. 2015;78(1–4):269–79.
[24] Natasha AR, Ghani JA, Haron C, Syarif J. The influence of machining condition and cutting tool wear on surface roughness of AISI 4340 steel. IOP Conf Ser Mater Sci Eng. 2018;290:012017.
[25] Lequien P, Poulachon G, Outeiro JC, Rech J. Hybrid experimental/modelling methodology for identifying the convective heat transfer coefficient in cryogenic assisted machining. Appl Therm Eng. 2018;128:500–7.
[26] Bag R, Panda A, Sahoo AK, Kumar R. Cutting tools characteristics and coating depositions for hard part turning of AISI 4340 martensitic steel: a review study. Mater Today Proc. 2020;26:2073–8.
[27] Li Y, Zheng G, Cheng X, Yang X, Xu R, Zhang H. Cutting performance evaluation of the coated tools in high-speed milling of AISI 4340 steel. Materials. 2019;12(19):1–16.
[28] Roy S, Kumar R, Das RK, Sahoo AK. A comprehensive review on machinability aspects in hard turning of AISI 4340 steel. IOP Conf Ser Mater Sci Eng. 2018;390(1).
[29] Chinchanikar S, Choudhury SK. Cutting force modeling considering tool wear effect during turning of hardened AISI 4340 alloy steel using multi-layer TiCN/Al_2O_3/TiN-coated carbide tools. Int J Adv Manuf Technol. 2016;83(9–12):1749–62.
[30] Natasha AR, Ghani JA, Che Haron CH, Syarif J, Musfirah AH. Temperature at the tool-chip interface in cryogenic and dry turning of AISI 4340 using carbide tool. Int J Simul Model. 2016;15(2):201–12.
[31] Umbrello D, Rotella G, Crea F. Experimental investigation of white layer formation in hard turning. AIP Conf Proc. 2011;1353:621–6.
[32] Wu Q, Miao W, Zhang Y, Gao H, Hui D. Mechanical properties of nanomaterials: a review. Nanotechnol Rev. 2020;9(1):259–73.
[33] Zhao Z, Qi T, Zhou W, Hui D, Xiao C, Qi J, Zheng Z. A review on the properties, reinforcing effects, and commercialization of nanomaterials for cement-based materials. Nanotechnol Rev. 2020;9(1):303–22.
[34] Liu C, Huang X, Wu Y, Deng X, Liu J, Zheng Z, Hui D. Review on the research progress of cement-based and geopolymer materials modified by graphene and graphene oxide. Nanotechnol Rev. 2020;9(1):155–69.
[35] Lin P, Hao Y, Zhang B. Strain rate sensitivity of Ti–22Al–25Nb (at%) alloy during high temperature deformation. Mater Sci Eng A. 2017;710:336–42.
[36] Duan M, Luo L, Liu Y. Microstructural evolution of AZ31 Mg alloy with surface mechanical attrition treatment: grain and texture gradient. J Alloys Compd. 2020;823:153691.
[37] Danilenko VN, Bachurin DV, Nazarov AA. Annealing-induced grain rotation in ultrafine-grained aluminum alloy. Rev Adv Mater Sci. 2018;55(1):69–77.
[38] Umbrello D, Rotella G, Matsumura T, Musha Y. Evaluation of microstructural changes by X-ray diffraction peak profile and focused ion beam/scanning ion microscope analysis. Int J Adv Manuf Technol. 2015;77(5–8):1465–74.
[39] Ginting A, Nouari M. Surface integrity of dry machined titanium alloys. Int J Mach Tools Manuf. 2009;49(3–4):325–32.
[40] Hassanpour H, Sadeghi MH, Rasti A, Shajari S. Investigation of surface roughness, microhardness and white layer thickness in hard milling of AISI 4340 using minimum quantity lubrication. J Clean Prod. 2016;120:124–34.
[41] Zhang F, Duan C, Sun W, Ju K. Effects of cutting conditions on the microstructure and residual stress of white and dark layers in cutting hardened steel. J Mater Process Technol. 2019; 266:599–611.
[42] Umbrello D, Pu Z, Caruso S, Outeiro JC, Jayal AD, Dillon OW, et al. The effects of cryogenic cooling on surface integrity in hard machining. Procedia Eng. 2011;19:371–6.
[43] Duan C, Zhang F, Sun W, Xu X, Wang M. White layer formation mechanism in dry turning hardened steel. J Adv Mech Des Syst Manuf. 2018;12:1–12.
[44] Kim W, Kwon P. Phase transformation and its effect on flank wear in machining steels. J Manuf Sci Eng. 2002;124(3): 659–66.
[45] Kaynak Y, Gharibi A, Yılmaz U, Köklü U, Aslantaş K. A comparison of flood cooling, minimum quantity lubrication and high pressure coolant on machining and surface integrity of titanium Ti-5553 alloy. J Manuf Process. 2018;34:503–12.
[46] Orlova TS, Skiba NV, Mavlyutov AM, Valiev RZ. Hardening by annealing and implementation of high ductility of ultra-fine grained aluminum: experiment and theory. Rev Adv Mater Sci. 2018;57(2):224–40.
[47] Rotella G, Imbrogno S, Candamano S, Umbrello D. Surface integrity of machined additively manufactured Ti alloys. J Mater Process Technol. 2018;259(2010):180–5.
[48] Mishra SK, Roy H, Lohar AK, Samanta SK, Tiwari S, Dutta K. A comparative assessment of crystallite size and lattice strain in differently cast A356 aluminium alloy. IOP Conf Ser Mater Sci Eng. 2015;75(1):2–8.
[49] Kong L, Zhou Y, Song K, Hui D, Hu H, Guo B, et al. Effect of aging on properties and nanoscale precipitates of Cu-Ag-Cr alloy. Nanotechnol Rev. 2020;9(1):70–8.
[50] Sun HQ, Shi YN, Zhang MX, Lu K. Plastic strain-induced grain refinement in the nanometer scale in a Mg alloy. Acta Mater. 2007;55(3):975–82.

[51] Jomaa W, Songmene V, Bocher P. An investigation of machining-induced residual stresses and microstructure of induction-hardened AISI 4340 steel. Mater Manuf Process. 2016;1–23.
[52] Pan Z, Tabei A, Shih DS, Garmestani H, Liang SY. The effects of dynamic evolution of microstructure on machining forces. Proc Inst Mech Eng Part B J Eng Manuf. 2018;232(14):2677–81.
[53] Liu ZQ, Ai X, Wang ZH. A comparison study of surface hardening by grinding versus machining. Key Eng Mater. 2009;304–305:156–60.
[54] Akcan S, Shah S, Moylan SP, Chhabra PN, Chandrasekar S, Yang HTY. Formation of white layers in steels by machining and their characteristics. Metall Mater Trans A Phys Metall Mater Sci. 2002;33(4):1245–54.
[55] Yang S, Umbrello D, Dillon OW, Puleo DA, Jawahir IS. Cryogenic cooling effect on surface and subsurface microstructural modifications in burnishing of Co–Cr–Mo biomaterial. J Mater Process Technol. 2015;217:211–21.
[56] Bukit N, Ginting EM, Hutagalung EA, Sidebang E, Frida E, Bunga F. Preparation and characterization of oil palm ash from boiler to nanoparticle. Rev Adv Mater Sci. 2019;58(1):195–200.
[57] Fan B, Wang J, Rao G. Influence of heat treatment method on grain-refining during warm deformation of medium carbon steel. Key Eng Mater. 2017;723:3–7.
[58] Mativenga PT, Mubashar A. White layer formation and tool wear in high speed milling of 57HRc tool steel using coated and uncoated tools. Int J Agil Syst Manag. 2015;2(2):172–85.
[59] Kompella S, Moylan SP, Chandrasekar S. Mechanical properties of thin surface layers affected by material removal processes. Surf Coatings Technol. 2001;146–147:384–90.
[60] Moylan SP, Kompella S, Chandrasekar S, Farris TN. A new approach for studying mechanical properties of thin surface layers affected by manufacturing processes. J Manuf Sci Eng. 2003;125:310–15.
[61] Chou YK. Surface hardening of AISI 4340 steel by machining: a preliminary investigation. J Mater Process Technol. 2002;124:171–7.
[62] Yue C, Liu X, Ma J, Liu Z, Liu F, Yang Y. Hardening effect on machined surface for precise hard cutting process with consideration of tool wear. Chinese J Mech Eng. 2014;27(6):1249–56.
[63] Zurita O, Di Graci V. Surface integrity in turning of annealed brass: hardness prediction. J Mater Eng Perform. 2012;21(7):1534–8.
[64] Ghani JA, Natasha AR, Hassan CHC, Syarif J. TRIZ approach for machining process innovation in cryogenic environment. Int J Mater Prod Technol. 2016;53(3/4):286–97.
[65] Guo YB, Warren AW. Microscale mechanical behavior of the subsurface by finishing processes. J Manuf Sci Eng. 2005;127(2):333–8.
[66] Imbrogno S, Rotella G, Rinaldi S. Surface and subsurface modifications of AA7075-T6 induced by dry and cryogenic high speed machining. Int J Adv Manuf Technol. 2020;107:905–18.
[67] Lampman S, Schneider MJ. Introduction to surface hardening of steels. in ASM Handbook, Volume 4A; 2013; vol. 4A. Ohio, USA. p. 389–98.
[68] Sirin SY, Sirin K, Kaluc E. Effect of the ion nitriding surface hardening process on fatigue behavior of AISI 4340 steel. Mater Charact. 2008;59(4):351–8.
[69] Sirin SY, Sirin K, Kaluc E. Influence of initial conditions on the mechanical behavior of ion nitrided AISI 4340 steel. Mater Sci Eng A. 2012;564:232–41.
[70] Grzesik W, Kruszynski B, Ruszaj A. Surface integrity of machined surfaces. Surface Integrity in Machining. London: Springer; 2010. p. 143–79.
[71] Maochuan G, Feng Z, Jinjia X, Shangyong Z, Sanjana SB, Junjie G, Ruoyu H. Surface modification of nano-sized carbon black for reinforcement of rubber. Nanotechnol Rev. 2019;8(1):405–14.
[72] Hu L, Qi W, Li Y. Coating strategies for atomic layer deposition. Nanotechnol Rev. 2017;6(6):527–47.
[73] Ali A, Phull AR, Zia M. Elemental zinc to zinc nanoparticles: is ZnO NPs crucial for life? Synthesis, toxicological, and environmental concerns. Nanotechnol Rev. 2018;7(5):413–41.